2-10-2021

Electromagnetic pollution alert: Microwave radiation and absorption in human organs and tissues

Nantakan Wongkasem
The University of Texas Rio Grande Valley

Recommended Citation

Wongkasem N. (2021). Electromagnetic pollution alert: Microwave radiation and absorption in human organs and tissues. Electromagnetic biology and medicine, 1–18. Advance online publication. https://doi.org/10.1080/15368378.2021.1874976

Electromagnetic Pollution Alert: Microwave Radiation and Absorption in Human Organs and Tissues

Nantakan Wongkasem*

Department of Electrical and Computer Engineering, College of Engineering and Computer Science, The University of Texas Rio Grande Valley, Edinburg 78539, Texas, USA
* Correspondence: nantakan.wongkasem@utrgv.edu

Abstract: Electromagnetic radiation from communication and electronic devices, networks, systems and base stations has drawn concern due to excessive global usage with increasing power and operating frequency level. Numerous previous researches only focus on how the radiation from certain frequency ranges of particular devices could harm specific human organs and tissues, resulting in distinct symptoms. In this research, electromagnetic propagation and properties in fourteen human organs and tissues were analyzed and investigated based on the organs and tissues' electromagnetic and mechanical parameters, and chemical composition. Counting the organs and tissues as electromagnetic materials, their permittivity and conductivity, computed by a 4-Cole-Cole mode, directly respective to the operating frequency, are interrelated to wave behavior and hence influence the organs' response.
Tests were conducted in 1GHz to 105GHz system settings, covering most microwave frequency uses: 2.4GHz of 4G-LTE, WiFi, Bluetooth, ZigBee, and the 5G ranges: 28GHz of 5G-mmW and 95GHz of 5G-IoT. Trial human organs and tissues were placed in the wave propagation direction of 2.4GHz and 28GHz dipole antennas, and a waveguide port operating from 95-105GHz. The quantitative data on the effects of 5G penetration and dissipation within human tissues are presented. The absorbance in all organs and tissues is significantly higher as frequency increases. As the wave enters the organ-tissue model, the wavelength is shortened due to the high organ-tissue permittivity. Skin-Bone-Brain layer simulation results demonstrate that both electric and magnetic fields vanish before passing the brain layer at all three focal frequencies of 2.4GHz, 28GHz, and 100GHz.

Keywords: electromagnetic; microwave; radiation; pollution; absorption; human organs; tissues; 5G.

1. Introduction

Electromagnetic (EM) spectrum in the radio frequency (RF) and microwave frequency ranges have been utilized for wireless communications since World War II (1939-1945). The radar frequency bands covering the EM spectrum according to IEEE standards are classified from High Frequency (HF), in the range of 0.003-0.03GHz (or 3-30MHz), to Millimeter (mm) in the range of 110-300GHz [1]. The frequency band usage is strictly regulated by each country's national laws and coordinated by the International Telecommunication Union (ITU) [2]. ITU regulations focus on the prevention of user, generation, and transmission interferences. Based on a global mobile data traffic forecast [3], by 2022, there will be 5.7 billion global mobile users, with the average smartphone generating 11GB of mobile traffic per month, and the video streaming accounting for 79% of the total mobile data traffic.

Based on their free-space radiation characteristics to serve numerous users in a wide-open space, wireless technologies require far more energy than wire technologies do. Although the energy efficiency of wireless access networks has been improving significantly, it still cannot keep up with rapidly increasing data usage and new functionalities at network level [4]. The available estimates of the internet energy intensity ranges from 136 kW/GB to 0.0064 kW/GB [5]. Setting the mid-point at 78kW/GB, we could consume circa 4.89 MW monthly worldwide in 2022 by mobile usage alone. Energy consumption of

wireless devices is directly connected to the device efficiency in both radiated or transmitter power and data speed. The transmitter power is rated based on a 0-dB antenna load of the receiving device or the portable transmitters, e.g. cell phones, internet of thing (IoT) wireless wearable units, smart home accessories, walkie-talkies, where the resistance and output of the received antenna are assumed to be exactly the same as those of the transmitter feeding it [6]. These portable transmitters can have a high radiated power when they are located close to their susceptible or broadcasting equipment. Typical field strengths from a handheld transmitter are 5V/m to 7V/m at 0.5m distance [7].

At a cellular tower or a cell site, an effective radiated power (ERP) of up to 500 watts per radio channel or transmitter, depending on the tower height, was permitted by the Federal Communications Commission (FCC) [8]. The majority of cellular or Personal Communications Services (PCS) cell sites in urban and suburban areas operate at an ERP of 100 watts per channel or less. An ERP of 100 watts corresponds to an actual radiated power of 5-10 watts, depending on the type of antenna used [9]. As with all forms of EM energy, the power density from a cellular or PCS transmitter decays proportionally to $1/R^2$ as the distance from the cell site increases. Therefore, for a common 40W of power density of about $10mW/m^2$ at 100m from the antenna tower, the power density will be $1mW/m^2$, as the distance increases to 300m away from the base station and the device will receive 1μW, based on the effective antenna area of $0.001m^2$. Having several mobile phones active in the same area, the total EM radiation can get close to 2W, the same level as the maximum power radiation of $5mW/cm^2$ at 2 inches from the microwave oven surface permitted by federal regulations [10]. Besides the aforementioned cellular emission, there is also EM radiation from wireless networks, smart and wearable devices, unceasingly scattering around, whether or not you are connected to their networks. Take for example the myriads of Wi-Fi connections in urban areas, or the in-flight Wi-Fi where anyone can video stream with a high data rate passing through their body. A few aircraft Wireless Local Area Network (WLAN) units, typically with a power of 30-50W per unit [11], are designed to deliver a good RF propagation within the aircraft cabins. Information on WLAN performance inside aircraft passenger cabins was initially studied by NASA in 2005 [12]. Moreover, according to the forecasts, in 2021 there will be 928 million connected wearable units worldwide [13]. These multi-millions of wireless devices and their enormous power consumption generate plenty of unused residual EM radiations all around us. In this research, we tag these unwanted and unnecessary EM radiations as '**Electromagnetic Pollution**' [14-17].

Radiated power varies with respect to the operating frequency and its system, depending mainly on different communication states, antenna types and RF circuits/networks. Figure 1 (a) presents the power consumption of different mobile phone parts [18-20]. The data communication measurements were focusing on Bluetooth (BT), WiFi and cellular with 3G technology. BT is widely used for short range communications and is commonly integrated in smart phones. The power value of 6 states: off, on, connected and idle, discovery, receiving and sending, were investigated [19]. While having the BT on, the power consumption increases by 3mW, from 12mW to 15mW. However, the power is close to 500mW when the BT is either in receiving or sending stage. Airpods and wireless headsets use BT for data communication. The power consumption of WiFi IEEE802.11 for infrastructure and ad hoc mode were measured in the range of 3-5m between the WLAN access point and a testing cellphone (Nokia N95). For the ad hoc mode, the power is about 1W with the phone in idle mode. Making or receiving video calls requires slightly more than 2W. It was shown that WiFi consumes 1.79 and 5.40 times more power than 3G while downloading and uploading with 1Mbps data speed, respectively [18]. The power consumption of devices used to access the internet is listed at 2.5W (tablet), 3W (mobile phone 4G LTE), 70W (Mid-range PC), 15W (Laptop) and 11W (Netbook) [20]. With the 5G technology, the data rate and capacity can be delivered up to 1000 times more than the 4G-LTE; however, in order to support the extra number of small cells and massive multiple-input multiple-output (MIMO) antennas, its energy consumption is rated approximately 1,000 times higher.

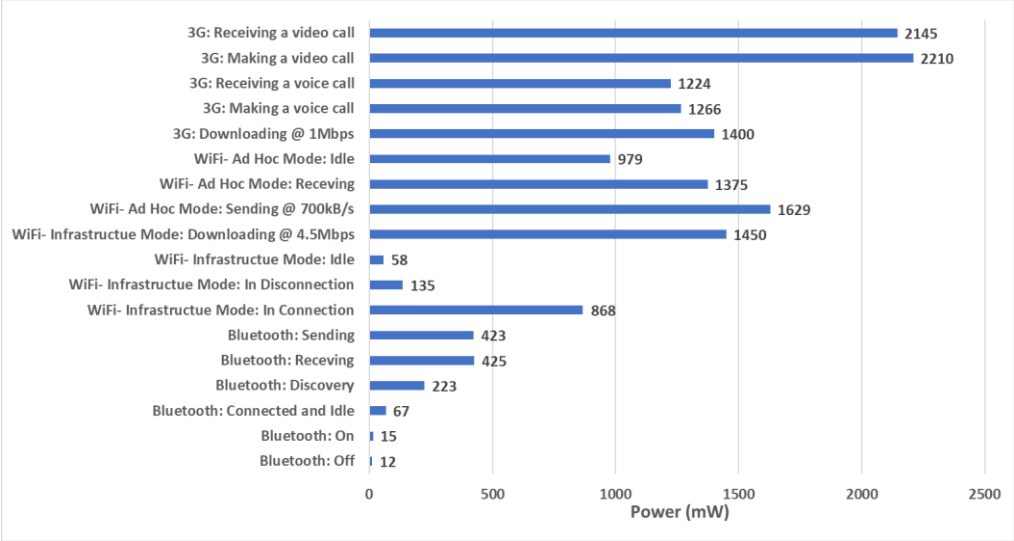

(**a**)

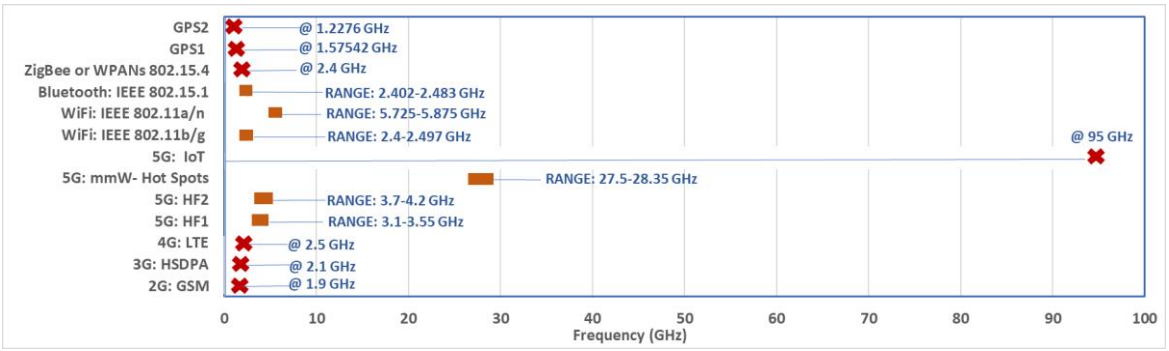

(**b**)

Figure 1. (**a**) Power consumption of different mobile phone parts [19]. (**b**) Communication system operating frequency of different band class indices.

Most commercial wireless RF communications operate within 2.5GHz, e.g. 2G: up to 1.9GHz, 3G: up to 2.1GHz, 4G: up to 2.5GHz, WiFi (IEEE 802.11 b/g): 2.4-2.497GHz, BT: 2.402-2.483GHz, ZigBee: up to 2.4GHz, etc. The maximum RF power of personal devices varies depending on the type of RF power class and the type of the over-the-air protocols, specified by device manufacturers, for example, 29-39dBm (power class 2-5) for GSM900, 23dBm (power class 3) for LTE. Although different technologies operate at the same frequency, their power consumption and radiation power can be diverse, depending on the communication range or distance, for example, less power consumption, BT (e.g. wireless headsets) covers less distance than ZigBee (e.g. wireless smart home accessories). The range of BT depends on its class, specified by its transmitting power. Primarily there are three classes of BT, Class 1-3, transmitting at 100mW, 2.5mW, and 1mW with a range of 100m, 10m, and fewer than 10m, respectively [21]. The ZigBee is designed to carry small amounts of data, with a maximum speed of 250kbps (WiFi has a max speed of 54Mbps), hence it consumes very little power, over a short distance with an average of 10-30m. As opposed to WiFi, with its mesh networking standard, each node in the network is connected to others, equalizing the coverage. It is important to stress that as the operating frequency gets higher, the power consumption is typically higher.

Figure 1 (b) presents the operating frequency of different band class indices. Besides the WiFi (IEEE 802.11a/n) which operates at 5.725-5.875GHz, all the 5G technologies work at much higher frequencies:

High Frequency 1 (HF1) at 3.1-3.55GHz, High Frequency 2 (HF2) at 3.7-4.2GHz, Millimeter Wave (mmW) Hot Spots at 27.5-28.35GHz, and Internet of Things (IOT) up to 95GHz.

According to Planck's equation: $E = hv$, the energy (E) of a photon particle is directly proportional to the frequency level (v), where the Planck constant (h) is fixed at $6.62607004 \times 10^{-34}$m^{2}kg/s. At lower operating frequency, for instance in the MHz range, the energy at the 10^{-6}eV produces only an induced current, hence there is non-ionizing radiation, yet it is not recommended to be exposed to machines operating in this range (e.g. magnetic resonance imaging (MRI) at 1-300MHz) too long and often [22]. Non-ionizing radiation is generated at frequencies below the ultraviolet regime, where $f < 10^{15}$Hz and $\mathrm{E} < 10$eV. This non-ionizing radiation corresponding to the energy level creates different elements and effects, i.e. 1) low currents ($f <$ Microwave), 2) high currents (f: Microwave-Infrared), and 3) electron excitations ($f >$ infrared). There are numerous applications operating within these frequency ranges, where non-ionizing radiation is unavoidably polluting. The thermal effects of RF radiation focusing on the absorption range and temperature elevation, from various mobile phone frequencies and different usage patterns, in the human head [23] and different human organs [24-25] were studied. It normally takes an extended time to track any long-term effects of these non-ionizing radiation on humans. Several short-term or even immediate side effects have been reported, including psychiatric effects (depression, anxiety, neurodegenerative issues), cardiac arrhythmias, tachycardia, fertility, affected eyesight or changed cell development, to name a few [26-43]. Similar to some serious diseases, where the symptoms do not show until they have already reached a certain stage, when the stray cells are completely saturated, the EM pollution has to be taken much more seriously, until it becomes irreparable. At ETHz, or 10^{18}Hz of the X-ray radiation, the energy can be as high as 10^{4}eV, considered as ionizing radiation, which can easily damage human DNA. To protect from this extreme harmful radiation, special materials, composed of high atomic mass elements, e.g. lead, bismuth, etc. [44] are used as shielding.

In this research we numerically analyze how human tissues, organs and fluids react with these EM pollutants, focusing primarily on the EM propagation and absorption. We do not draw a conclusion on the extent of human related damage [26-43]. We investigate how human organs, tissues, and fluids react, while resonated by the EM excitation or radiation in the microwave ranges from 1GHz to 105GHz, focusing on the communication frequencies of 2.4GHz (4G-LTE, Wi-Fi, ZigBee, Bluetooth, etc.), 28GHz (5G-mmW) and 95GHz (5G-IoT). Dispersive EM parameters, including thermal and mechanical parameters, and chemical element contents of human organs and tissues are discussed. The EM propagation properties and absorbance of the organs, tissues, and fluids from the EM emission are also closely observed. A commonly used antenna type, 2.4GHz and 28GHz dipole, is employed to launch the EM source to investigate electric (E) and magnetic (H) fields propagating inside human organs and tissues. The organs and tissues are also tested with a 95-100GHz waveguide port. Three broad frequency ranges of 1-4GHz, 23-33GHz, and 95-105GHz are set up to further investigate the absorbance, transmittance, and reflectance in studied organ and tissue models including far-field radiation. An example of layered structure: skin-bone-brain, is studied focusing on E-field and H-field intensity propagating and absorbing in each layer. CST Microwave Studio [45] is implemented for the real-time simulations.

2. Water Content, Elemental Composition and Electromagnetic Properties of Human Tissues

All human tissues, organs and fluids, except bones, contain more than 70% water. What they have in common is the high percentage of Hydrogen (H), Oxygen (O), and C (Carbon), with Nitrogen (N), Sodium (Na), and Magnesium (Mg) found in most organs. Human organs and tissues, % water content [46-47], % element composition, thermal conductivity, heat transfer rate, and heat generation rate are listed in Table 1 [48].

Table 1. Water content, elemental composition, thermal conductivity, heat transfer/generation rates of different human organs and tissues [46-48].

Human Organs and Tissues	Water Content (%)	Elemental Composition (%)						Thermal Conductivity (W/m/°C)	Heat Transfer Rate (ml/min./kg)	Heat Generation Rate (W/kg)
		H	C	N	O	Na	Mg			
Blood	93.33	60	10	1.3	28	0.037	0.0005	0.52	10000	0
Bone (Cancellous)	31.81	43	14	3.3	30	0.025	0.094	0.31	30	0.46
Brain (including Spinal Cord and Nerve Trunks)	73.33	65	6.2	0.57	27	0.048	0.0037	0.51	559	11.37
Breast	NA	50	37	0.30	13	0.018	0	0.21	47	0.73
Eye (Lens)	NA	61	10	2.5	26	0.014	0	0.43	0	0
Eye (Retina)	NA	-	-	-	-	-	-	0.55	240	4.89
Gallbladder	NA	-	-	-	-	-	-	0.52	30	0.46
Heart Lumen	73.69	60	10	1.3	28	0.037	0.0005	0.52	10000	0
Heart Muscle	NA	64	7.2	1.3	28	0.027	0	0.56	1026	39.45
Kidneys	79.47	63	6.9	1.3	28	0.054	0	0.53	3795	18.05
Large Intestine	NA	64	7.1	1.3	28	0.027	0	0.54	765	11.85
Liver	71.46	63	7.3	1.3	28	0.054	0	0.52	860	9.93
Lungs (Inflated)	83.74	64	5.3	0.71	30	0.053	0.0095	0.39	401	6.21
Muscle	79.52	63	6.9	1.5	28	0.025	0.0020	0.49	37	0.91
Skin	64.68	62	1.1	1.9	25	0.041	0.00038	0.37	106	1.65
Spleen	78.69	64	5.9	1.4	29	0.027	0	0.53	1557	24.11
Urinary Bladder Wall	NA	64	4.9	1.1	29	0.054	0	0.52	78	1.21
Air	NA	0	0.015	78	21	0	0	0.026 (at 30C)	0	0
Water	NA	67	0	0	33	0	0	0.60	0	0

The water content of 93.33% in liquid tissues (blood) is the highest, followed by lungs (83.74%), kidneys (79.47%), and muscles (79.52%). The brain has the highest content of H, while C, N, and O, are found highest in breast, bone, and lungs, respectively. Thermal conductivity, heat transfer rate, and heat generation rate are the highest in the heart. The correlation between these parameters and the EM propagation and absorbance is investigated.

EM materials can be fundamentally classified as conductor, dielectric and magnetic materials, and free-space, based on their EM properties, i.e. complex permittivity ($\varepsilon = \varepsilon' + j\varepsilon''$) and complex permeability ($\mu = \mu' + j\mu''$), specified at their operating frequency ($f = \frac{\omega}{2\pi}$). Loss tangent, the ratio of the real part of the permittivity and the imaginary part of the permittivity is connected to the material's conductivity: $tan\theta = \frac{\varepsilon''}{\varepsilon'} = \frac{\sigma}{\omega\varepsilon}$. The conductivity value (σ, S/m) is commonly used to discern if the material is either a lossless

($\sigma \ll \omega\varepsilon$ or small θ) or a lossy ($\sigma \gg \omega\varepsilon$ or large θ) dielectric. Due to conductors extreme conductivity and hence high dielectric loss (ε''), waves almost totally reflect back when reaching the conductor surface, while some can penetrate inside the conductor with the distance, $\delta = \frac{1}{\sqrt{\pi f \mu \sigma}}$, defined as skin depth or penetration depth. At δ, the wave amplitude is attenuated by the factor e^{-1}or about 37% of its original peak. Contrasting to conductors, waves can always propagate passing dielectric materials, depending on the attenuation constant, α. Figure 2. presents the real part of the permittivity (ε') and conductivity (σ) of human organs and tissues at radio and microwave frequencies, from 100MHz to 100GHz, computed by a 4-Cole-Cole model [47-48], where the spectrum extends from Hz to GHz and shows 4 dispersion regions. The complex permittivity of the model, described in Equation (1), was specifically derived for the frequency dependence of the dielectric properties of the investigated tissues [48].

$$\varepsilon(\omega) = \varepsilon' + j\varepsilon'' = \varepsilon_\infty + \sum_{n=1}^{4} \frac{\Delta\varepsilon_n}{1+(j\omega\tau_n)^{(1-\alpha_n)}} - \frac{j\sigma_i}{\omega\varepsilon_0} \qquad (1)$$

in which, ε_∞ is the permittivity in the THz range, and σ_i is the ionic conductivity, for each dispersion region. τ is the relaxation time and $\Delta\varepsilon$ is the drop in permittivity in the frequency range corresponding to $1 \gg \omega\tau \gg 1$. With a choice of parameters appropriate for each tissue, Equation (1) corresponding to the whole spectrum, could be used to predict its dielectric behavior over the desired frequency range.

It is important to stress that in order to improve the accuracy of the complex permittivity values of any water-based materials, the ionic conduction should be applied to the Cole-Cole model [49], as the dielectric properties are strongly related to the molecular dynamics of dipoles and charges, for both ions and electrons, under any oscillating EM fields. Here, the dielectric losses were assumed to be induced by conduction processes. This simplifying hypothesis is valid, as biological media such as tissues contain many ions, unlike pure water in which dielectric relaxation is the predominant mode of dissipation around 18GHz. Hence, both the molecular dynamics of dipoles and charges under EM fields, as well as the degree of the EM wave susceptibility of the material, are taken into account while obtaining the dielectric properties of a material [49-53].

Based on the aforementioned 4-Cole-Cole model, the relative permittivity of all listed organs and tissues decreases exponentially with an e^{-x} function, below 10, at 100GHz. The top 5 permittivity values, from high to low, come from: gall bladder, heart lumen, breast (gland), heart muscle, and muscles. The lowest values are seen in breast (fat), bones (cancellous), urinary bladder wall, lungs, and eye retina. On the other hand, the conductivity increases exponentially with a $-e^{-x}$ function. The imaginary part of the permittivity is linked to the conductivity: $\varepsilon'' = \frac{\sigma(\omega)}{\omega\varepsilon_0}$. The order of organs and tissues regarding to their conductivity values is almost identical to the organ order, considering the permittivity values. At higher frequency, the permittivity and conductivity of all organs and tissues is lower and higher, respectively, resulting in a higher attenuation constant, which leads to less transmission and more absorption. These EM parameters are added in the CST material database, where only the values up to 3GHz are provided.

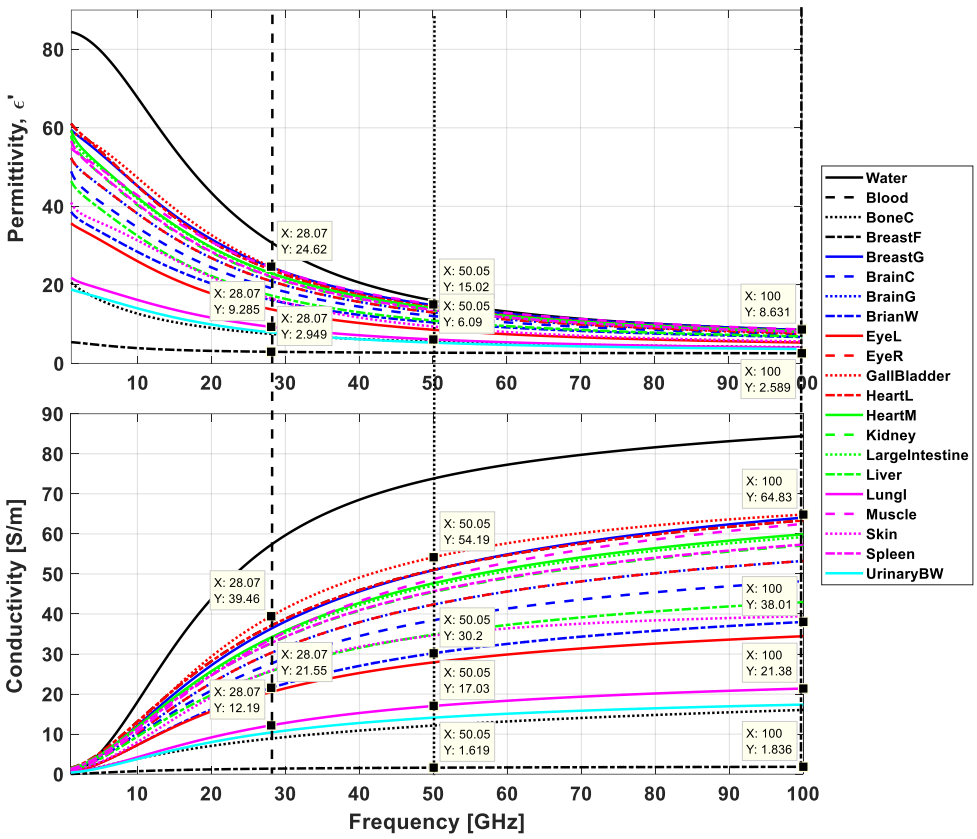

Figure 2. Permittivity and conductivity of human tissues and organs calculated from 100MHz to 100GHz [47-48].

3. Electromagnetic Propagation in Human Tissues and Organs

Waves propagate without any attenuation in lossless materials, for example, free-space or vacuum. However, in general, there is always loss in materials, where the electric (E-) and magnetic (H-) field of any transverse EM (or TEM) mode can be calculated from:

$$\vec{E}(z,t) = E_0 e^{-\alpha z} \cos(\omega t - \beta z)\vec{a}_x \tag{2}$$

$$\vec{H}(z,t) = \frac{E_0}{|\eta|} e^{-\alpha z} \cos(\omega t - \beta z - \theta_\eta)\vec{a}_y \tag{3}$$

These time-varying E- and H-fields are the main EM components, where their resonating directions ($\vec{a}_x$ of $\vec{E}$ and $\vec{a}_y$ of $\vec{H}$), create an EM wave propagating in the direction $\vec{a}_z = \vec{a}_x \times \vec{a}_y$. Wave propagation properties are analyzed by the materials' propagation constant: $\gamma = \alpha + j\beta$, where $\alpha = \omega\sqrt{\frac{\mu\varepsilon}{2}\left[\sqrt{1+\left[\frac{\sigma}{\omega\varepsilon}\right]^2}-1\right]}$ and $\beta = \omega\sqrt{\frac{\mu\varepsilon}{2}\left[\sqrt{1+\left[\frac{\sigma}{\omega\varepsilon}\right]^2}+1\right]}$ are the attenuation and phase constant, and $\eta = \sqrt{\frac{j\omega\mu}{\sigma+j\omega\varepsilon}} = |\eta|\angle\theta_\eta$ is the intrinsic impedance.

The incident radiation, or the excitation wave, and the object, or scatter, with which the radiation interacts, are the two main elements for the formulation of a scattering problem [54], interrelated with propagation properties. Based on the Lorenz-Mie theory [55-57], the incident radiation is corresponded to

the wave properties, including wave format and environment, while the material and size are the key contributions of the observed scatter.

We demonstrate experiments focusing on 3 main operating frequencies: 2.4GHz, 28GHz, and 100GHz, where trial human organs and tissues are placed in A) a wave propagation direction of 2.4GHz and 28GHz dipole antennas, and B) a waveguide port operating from 95-105GHz.

3.1. Organs and tissues placement facing 2.4GHz and 28GHz dipole antennas

A half-wavelength 2.4GHz dipole antenna and a half-wavelength 28GHz dipole antenna are individually placed in front of a human organ or tissue model in an 80mm (for the 2.4GHz model) and a 20mm (for the 28GHz model) diameter spherical shape. The perfectly matched layer (PML) or open 'add space', a specific CST name, set for the system boundaries, ensures the least reflected and scattered waves from the boundaries. The estimated reflected level is 0.0001 or 0.01%. The dipole antenna is assigned as Port 1, the transmitting port, 42.5mm or 0.34λ (the 2.4GHz dipole), and 10.7mm or 1λ (the 28GHz dipole) from the observation organ or tissue. The distance is chosen as an example of users holding or carrying a cellphone, tablet, wireless earbuds, smart watch, etc., as well as to ensure a full-wave propagation. Figure 3 shows the physical domain of the 2.4GHz and 28GHz dipole set-ups with the dimensions and boundaries.

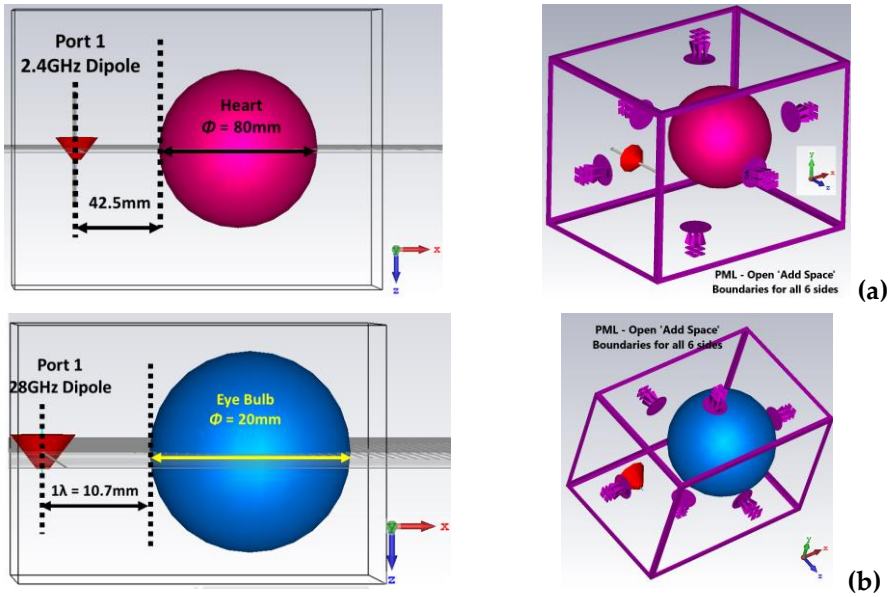

Figure 3. (a) 2.4GHz and (b) 28GHz dipole antenna placed in front of a human organ, where PML boundaries are set at all 6 sides.

Figure 4 presents the 3D radiating E- and H-field at a center-cut plane, captured at 2.4GHz and 28GHz from the aforementioned dipoles. The top-view displays the wavefront, where the operating wavelength and field intensity can be observed. As the wave enters the organ and tissue model, where the complex permittivity is much higher than that of air or free space, the wavelength is clearly shortened, approximately by 5-8 times. This is based on the relationship between the material EM properties and TEM (Transverse EM mode) propagation phase velocity: $v_p = \frac{\omega}{\beta} = \sqrt{\frac{1}{\varepsilon_0 \varepsilon_r \mu_0 \mu_r}}$. Therefore, the wave is somewhat accelerating, while it is propagating through and oscillating inside organs and tissues. If the excitation frequency and power is higher, the organs and tissues will need to be tolerating a much higher stimulation. Any dielectric material becomes conducting when the applied E-field is so high and breaks down the dielectric strength. The same E- and H-field intensity scale for all models is set in a range of 5e+3V/m to 5e-

6 V/m and 10 A/m to 1e-6A/m. The 2D maximum E-field is in the range of 9,500-9,600 V/m (of the 2.4GHz), and of 101,700-101,900 V/m (of the 28GHz), while the 2D maximum H-field is in the range of 14.20-14.35 A/m (of the 2.4GHz), and of 173-174 A/m (of the 28GHz). The lowest propagation frequency (or longest wavelength) is found in the lung model, where permittivity is lowest at 20.510+j5.9168 and 4.002+j21.384 at 2.4GHz and 28GHz, respectively.

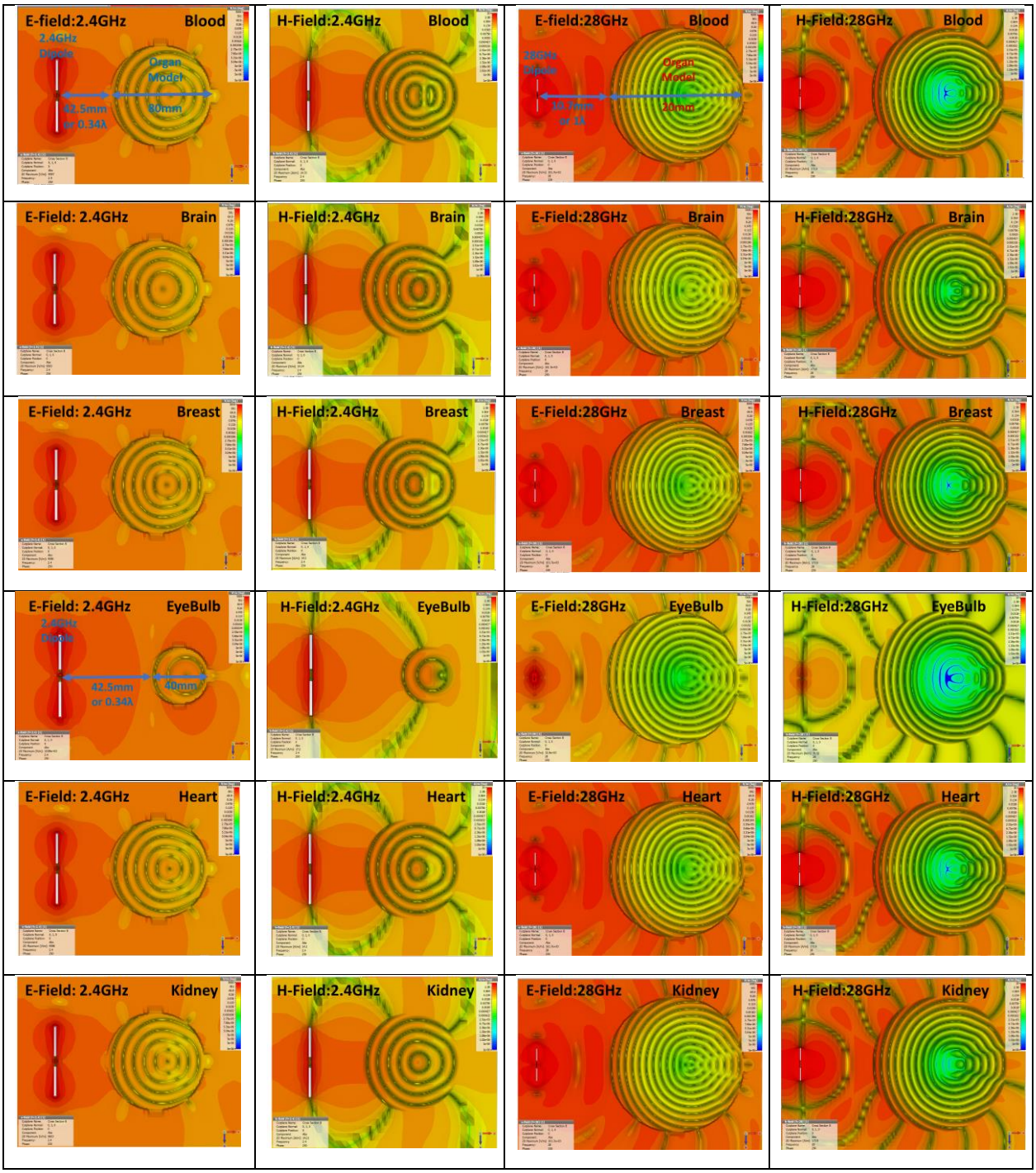

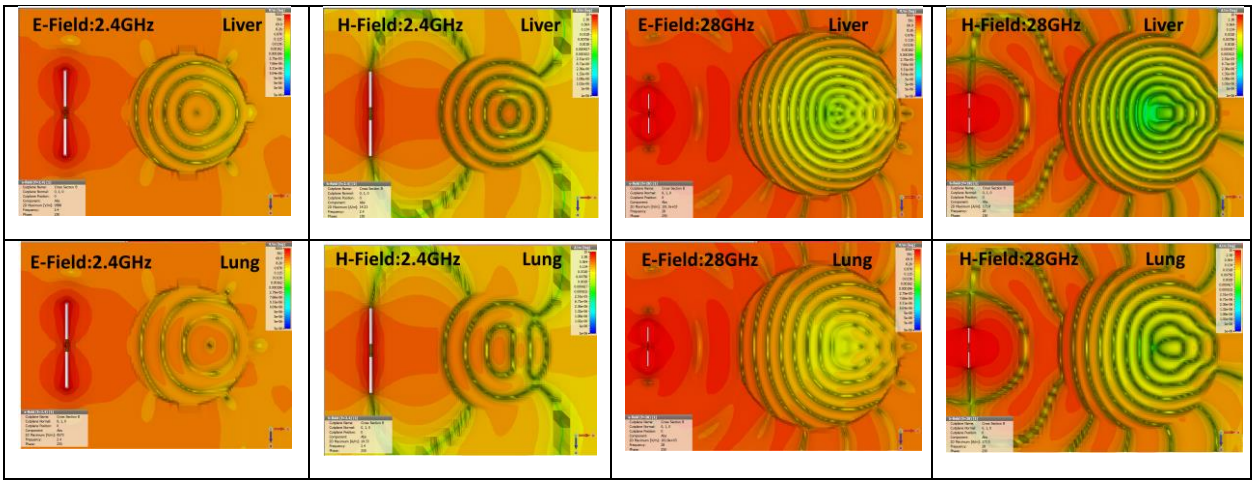

Figure 4. E-and H-fields: 3D center-cut plane in organ models from 2.4GHz and 28GHz dipoles.

3.2. Organs and tissues placement in front of a 95-105GHz waveguide port

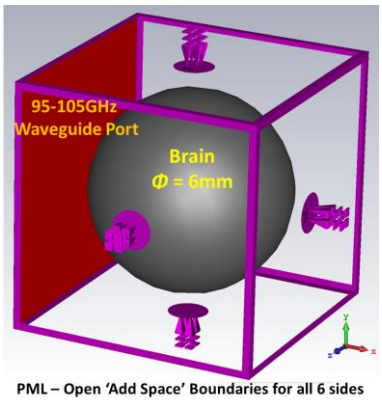

Figure 5. Brain model placed in front of a 95-105 waveguide port, where PML boundaries are set at all 6 sides.

The observed organ or tissue model in a 6mm diameter spherical shape is placed in front of a waveguide port, where an excitation is launched to investigate EM propagation in a broad high frequency range of 95GHz-100GHz, shown in Figure 5. The PML boundaries are set for the system to ensure the least reflected and scattered waves from the boundaries. The estimated reflected level is 0.0001 or 0.01%. The distance from the port to the model is automatically set by CST to ensure a full plane wave propagation.

As illustrated in Figure 6(a), the 2D maximum E-field intensity increases significantly as the EM source frequency increases, e.g. 3,656 V/m at 95GHz, 3,708 V/m at 100GHz, and 3,804 V/m at 105GHz in the brain model, or 5,161 V/m at 95GHz, 5,277 V/m at 100GHz, and 5,378 V/m at 105GHz in the lung model. The increasing intensity level from 95GHz to 105GHz radiation in this setting is in between 3.89% (brain) and 4.86% (liver). The 2D maximum H-field intensity is quite stable, but shows a slight increase inclination at higher frequency. The field intensity decreases as the wave propagates through the model, indicating a wave attenuation from the material absorption, as shown in Figure 6(b). The H-field is 12.88 A/m when it enters the eye bulb model at the plane x = -2 and reduces to 2.587 A/m at x = +2. The next section focuses on the absorbance study

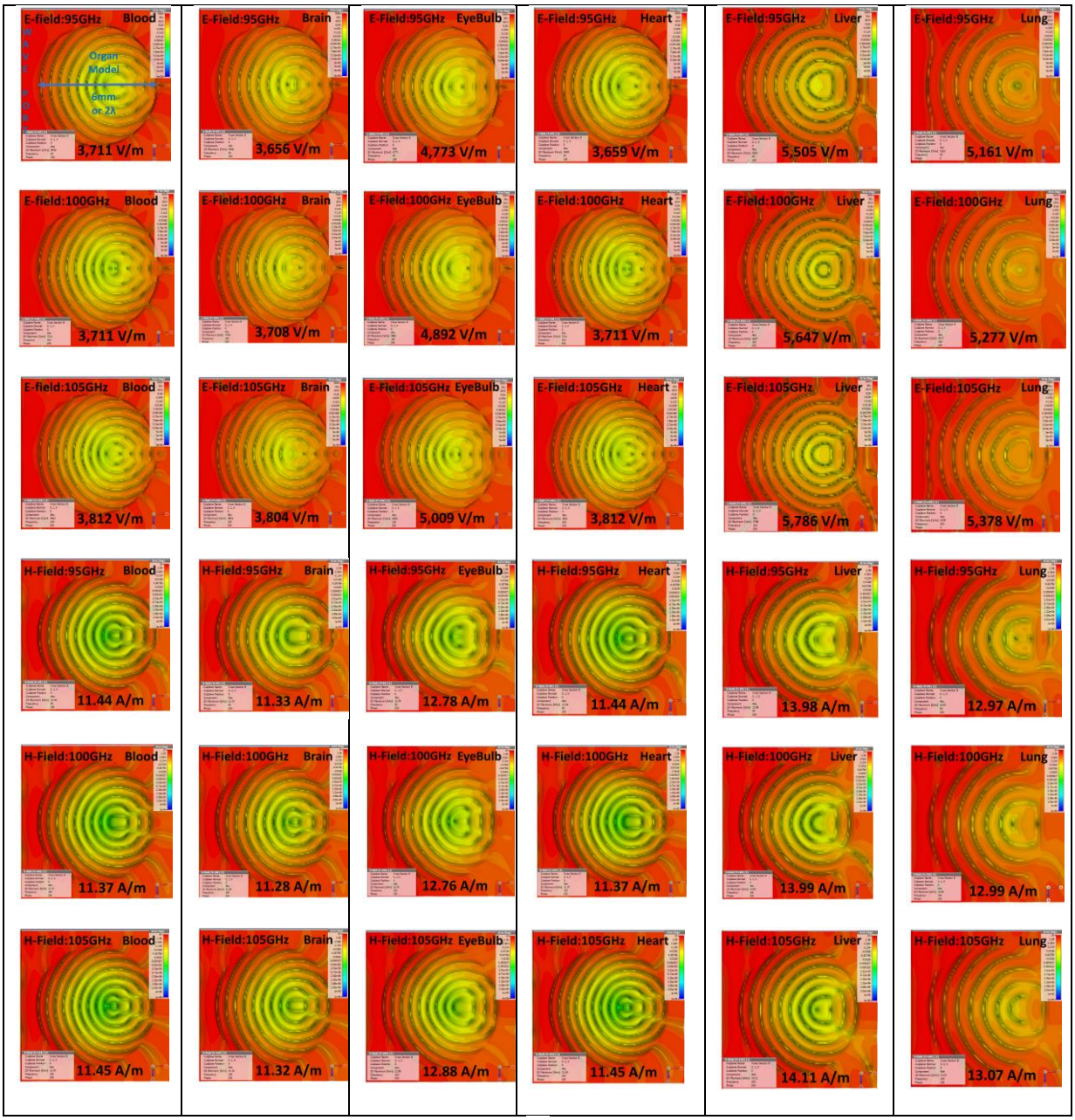
E-field:95GHz Blood
Organ Model
6mm or 2λ
3,711 V/m
E-Field:95GHz Brain
3,656 V/m
E-Field:95GHz EyeBulb
4,773 V/m
E-Field:95GHz Heart
3,659 V/m
E-Field:95GHz Liver
5,505 V/m
E-Field:95GHz Lung
5,161 V/m
E-field:100GHz Blood
3,711 V/m
E-Field:100GHz Brain
3,708 V/m
E-Field:100GHz EyeBulb
4,892 V/m
E-Field:100GHz Heart
3,711 V/m
E-Field:100GHz Liver
5,647 V/m
E-Field:100GHz Lung
5,277 V/m
E-Field:105GHz Blood
3,812 V/m
E-Field:105GHz Brain
3,804 V/m
E-Field:105GHz EyeBulb
5,009 V/m
E-Field:105GHz Heart
3,812 V/m
E-Field:105GHz Liver
5,786 V/m
E-Field:105GHz Lung
5,378 V/m
H-Field:95GHz Blood
11.44 A/m
H-Field:95GHz Brain
11.33 A/m
H-Field:95GHz EyeBulb
12.78 A/m
H-Field:95GHz Heart
11.44 A/m
H-Field:95GHz Liver
13.98 A/m
H-Field:95GHz Lung
12.97 A/m
H-Field:100GHz Blood
11.37 A/m
H-Field:100GHz Brain
11.28 A/m
H-Field:100GHz EyeBulb
12.76 A/m
H-Field:100GHz Heart
11.37 A/m
H-Field:100GHz Liver
13.99 A/m
H-Field:100GHz Lung
12.99 A/m
H-Field:105GHz Blood
11.45 A/m
H-Field:105GHz Brain
11.32 A/m
H-Field:105GHz EyeBulb
12.88 A/m
H-Field:105GHz Heart
11.45 A/m
H-Field:105GHz Liver
14.11 A/m
H-Field:105GHz Lung
13.07 A/m

(a)

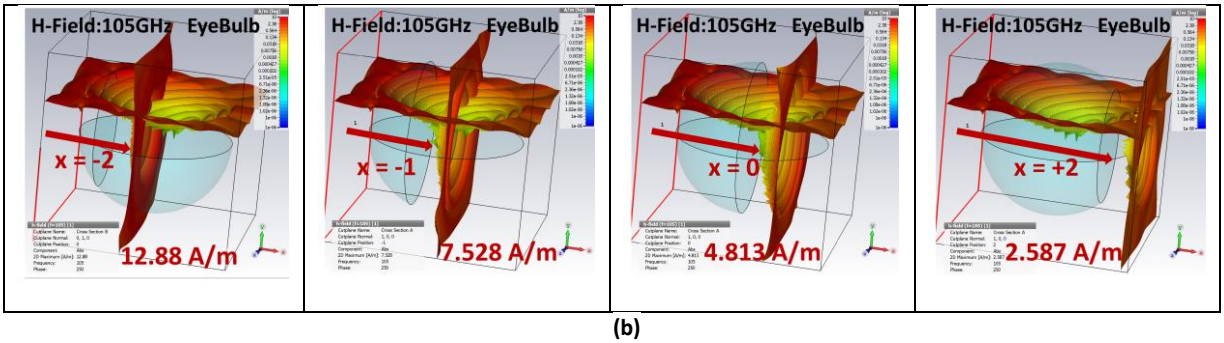
H-Field:105GHz EyeBulb
x = -2
12.88 A/m
H-Field:105GHz EyeBulb
x = -1
7.528 A/m
H-Field:105GHz EyeBulb
x = 0
4.813 A/m
H-Field:105GHz EyeBulb
x = +2
2.587 A/m

(b)

Figure 6. (**a**) E-and H-fields: 3D center-cut plane in organ models from a 95-100GHz waveguide port.(**b**) 3D center-cut plane (y = 0) H-field at 105GHz of eye bulb at x = -2, -1, 0, and 2mm.

4. Electromagnetic Absorption in Human Tissues and Organs

Waves are weakening or attenuating while propagating in any lossy materials, where $\alpha \neq 0$, which directly corresponds to the material conductivity and the imaginary of the of permittivity. The attenuation constant therefore indicates material loss or absorption. Since human organ and tissue conductivity increases exponentially as the frequency increases, for example: σ_{Brain} = 0.790, 2.069, 27.570, and 48.194S/m at 100MHz, 2.4GHz, 28GHz, and 100GHz, respectively, besides the higher power and E- and H-field strength, our organs and tissues are also dealing with higher absorption at higher frequency levels.

EM absorbance ($A(\omega)$) in materials is defined by the amount of residual waves in materials, excluding the transmitting and reflected waves, where their field strength is defined as transmittance ($T(\omega)$) and reflectance ($R(\omega)$.), respectively. Based on the wave propagation theory, the transmittance and reflectance are respectively obtained from the scattering parameters, i.e. the transmission coefficient (S_{21}) and reflection coefficient ((S_{11})). Equation 3 presents the relationship among the absorbance, transmittance, and reflectance in terms of the scattering parameters:

$$A(\omega) = 1 - T(\omega) - R(\omega) = 1 - |S_{21}|^2 - |S_{11}|^2 \quad (1)$$

The absorbance, transmittance and reflectance of any material depend directly on the operating frequency ($\omega = 2\pi f$). It means that the same material behaves electromagnetically different while being excited by waves of different frequencies. At one frequency, the EM waves can simply propagate through a material without any lingering in the material, at another frequency they can resonate heavily in the material with very high absorbance, and at other frequency, they can all be reflected back to the launching source.

To test them for the EM absorption, organ and tissue models in flat shape with infinite surface (width and length) are placed in between two waveguide ports, operating in 3 different frequency bands. A special skin-bone-brain layer case is also investigated.

4.1. Flat shape organ and tissue model with infinite surface placement in between waveguide ports

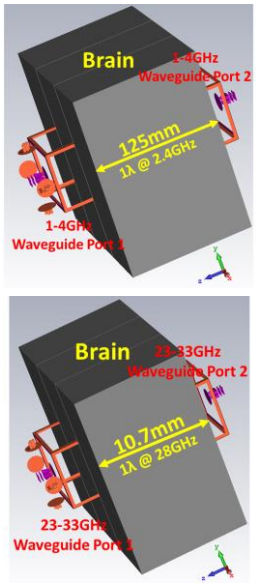

Organs and tissues are examined by flat shape structure analysis. The studied model is placed in between two waveguide ports, where port 1, Z_{min}, and port 2, Z_{max}, are the transmitting and receiving port, respectively, as shown in Figure 7. The 1-4GHz and 23-33GHz waves are launched from the Z_{min} location toward the Z_{max} port in the +z radiation direction. These EM waves are created by the E_y and H_x components for a standard free space propagation, TEM mode. The heart, brain, and lung, selected based on their EM parameters (Table 1 and Figure 2), with a finite 125mm and 10.7mm thickness (along the z axis), or one wavelength of 2.4GHz and 28GHz, and an infinite x-y plane (perpendicular to the excitation) set by the periodic boundaries, are modeled for this full-wave analysis. This setting is designed to investigate the absorbance, transmittance and reflectance of the human organs and tissues.

Figure 7. Brain placed in between (a) 1-4GHz and (b) 23-33GHz waveguide ports along z-axis, where periodic boundaries are set in x- and y- axes.

Significantly higher E- and H-field intensity, around 10 times, are observed in the three organs as the operating frequency increases from 2.4GHz (4G-LTE) to 28GHz (5G-mmW), presented in Figure 8. These higher values are not exact numbers, but are directly connected to their power requirement for any higher frequency systems/networks. Similar to the previous propagation demonstration, the EM wavelength inside the organs is shortened (higher frequency). The cut-plane E- and H-fields along the propagation direction are dramatically attenuated and vanish before passing the models. The transmittance (solid line) of the three organs is significantly low in the e-3 level in the 1-4GHz range and the e-5 level in the 23-33GHz range. The absorbance (dotted line) is found the highest in the lung, i.e. 66.49% at 28GHz and 58.69% at 2.4GHz, while the lowest is in the heart, i.e. 47.24% at 28GHz and 39.83GHz. These great absorbance values contribute to its inflated structure, in majority composed of air. Its complex permittivity, conductivity, material density (1020 Kg/m^3), blood flow coefficient (9,500 W/K/m^3), as well as Basel metabolic rate (1,700 W/m^3), is the lowest among all observed models [38]. On the other hand, the heart reflects the large portion of the waves in both frequency ranges approximately at 50% and 60%, respectively. It is also linked to its higher EM dispersion, thermal, mechanic, and density values.

The transmittance and reflectance also indicate the scattering behavior and multiple absorbing possibility, as the wave can transmit to, reflect from other tissues and organs, and then launch back onto other organs or tissues. Further investigation on complex models where a set of tissues and organs are integrated will definitely provide more information on this matter.

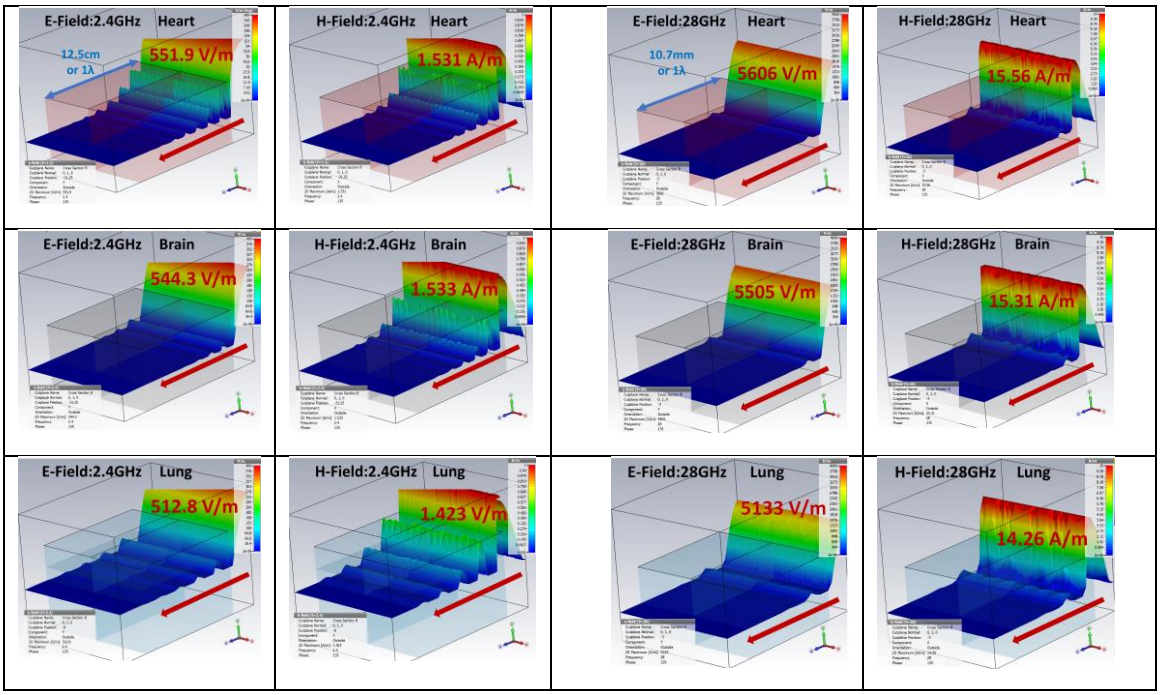

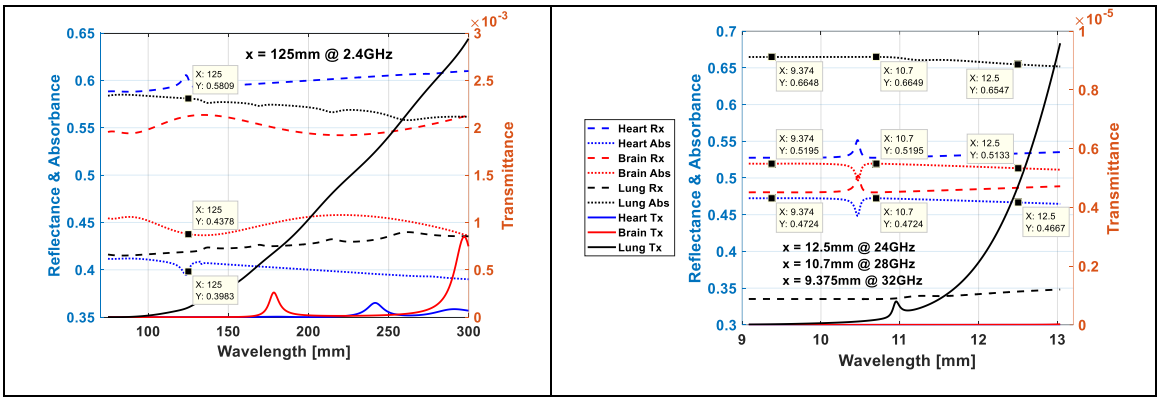

Figure 8. Top: E-and H-fields: 3D center-cutting plane in organ models in between 1-4GHz and 23-33GHz waveguides. Bottom: Transmittance (solid line), reflectance (dashed line) and absorbance (dotted line) of heart, brain, and lung in the 1-4GHz and 23-33GHz ranges.

14 organ and tissue models are tested for their absorbance, reflectance, and transmittance in the 95-105GHz range. The models with the finite 2cm thickness and an infinite x-y plane (perpendicular to the excitation) are created for EM full-wave analysis. The absorbance is found greater than 60% in all models, and higher as the frequency increases, shown in Figure 9-top. At 100GHz, bone (83.01%), urinary bladder wall (82.95%), lung (80.02%), liver (68.18%), brain (66.18%), and eye (64.46%) are the highest absorbing organs. The rest of the EM field is mostly reflected, as the transmittance values are extremely low, below the e-20 level. The absorbance increases significantly as the frequency increases, e.g. in the brain model, the absorbance is 43.78% at 2.4GHz, 51.95% at 28GHz, and 66.16% at 100GHz. Figure 9-bottom presents the far-field pattern through bone, brain, and heart. A green-yellow-red balloon indicates the EM strength along the propagation directly, easily noticed by the radius and color intensity. The radiation efficiency (Rad. Eff.) at -6.894dB (bone), -2.919dB (brain), and -2.023dB (heart) is observed. The low negative values of the radiation efficiency reflect the low or poor transmission between the transmitting and receiving port, indicating high loss or absorption in the organ. The total radar cross section (RCS) of bone (-58.16dBm^2), brain (-55.17dBm^2), and heart (-54.60dBm^2) is also measured. RCS is a property of the target's reflectivity. A low negative RCS value indicates low reflected wave intensity. The RCS is directly correlated with the reflectance. The highest reflectance is 38.8%.

Based on this data, there is no clear correlation between the EM absorbance and heat transfer and generation rate (Table 1). Contrastingly, the absorbance is highly connected with the permittivity and conductivity. The top five highly EM absorbing organs all have low complex permittivity and conductivity.

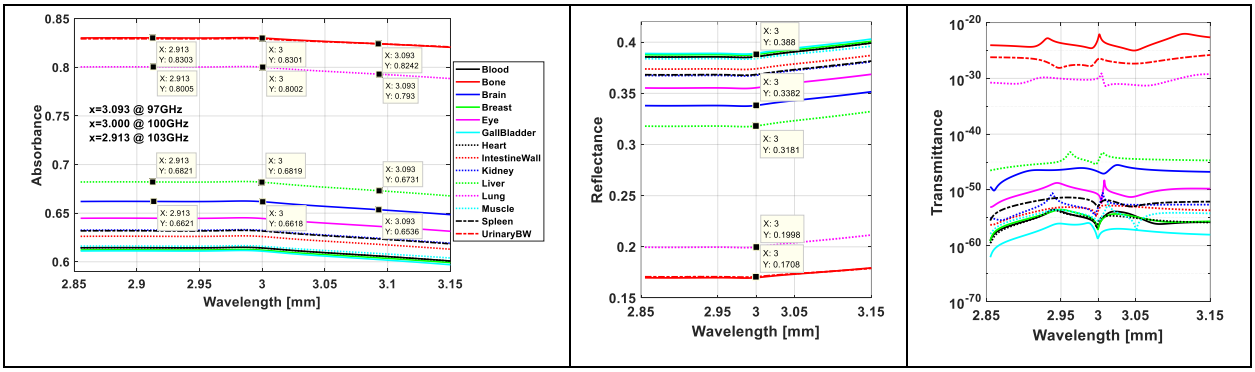

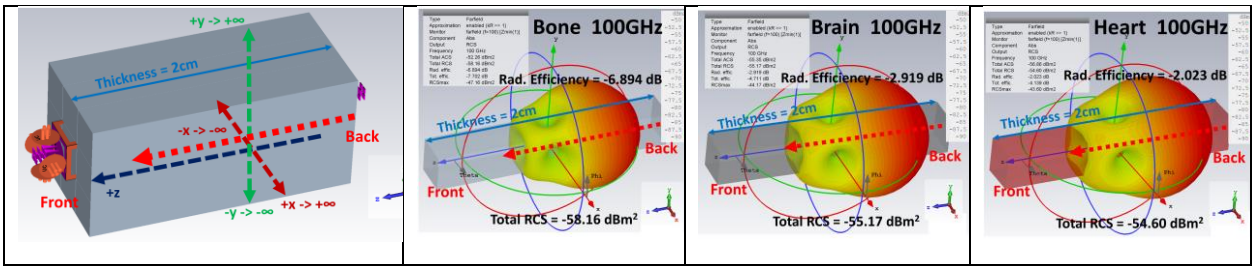

Figure 9. Top: Absorbance, reflectance, and transmittance of 13 organ and tissue models in 95-105GHz range. Bottom: System setting and far-field radiation at 100GHz through a 2cm layer of bone, brain, and heart.

4.2. Skin-Bone-Brain layer placement in between waveguide ports

A flat uniform layer of 0.12mm skin (Avg. face skin thickness), 6mm bone, and 60mm brain is tested for E-field and H-field propagation, as well as EM absorption, by placing it in between the 1-4GHz, 23-33GHz, and 95-105 waveguide ports. The infinite structure plane is set perpendicular to the excitation. Therefore, the transmitting wave (Back) from the transmitting port will perceive the layer model, in the Skin-Bone-Brain order, as an infinite plane with finite thickness. The distance from the ports to the layer is set for full plane wave excitation.

As shown in Figure 10-left, the propagating E- and H-fields are hardly passing through the bone layer at all 3 frequencies, and all disappear inside the brain layer. This observation is confirmed by the E-field and H-field values recorded behind the skin, bone, and brain layer at Probes 1-4, presented in Figure 10-middle. It is clearly shown that both the E-field and H-field are highly absorbed inside each layer at higher frequencies. As one said, 'nature does nothing uselessly', the skin and the bone layers do indeed protect our brain: at 28GHz, the E-field of 1326 V/m and H-field of 11.92 A/m in the middle of the skin layer are reduced to 238.8 V/m and 1.93 A/m at the middle of the bone layer, before entering the brain, or at a 82.0% (E-field) and 83.8% (H-field) decreasing rate. At 100GHz, the E- and H-fields are lessened by almost 99%. However, as there is almost no E-field and H-field radiating passed the brain layer, all the remaining EM-field remains inside the brain. As shown in Figure 10-right, the overall layer absorbance (dotted line) is greatly elevated at all 3 frequencies at 69.18% (2.4GHz), 65.69% (28GHz), and 71.49% (100GHz). The reflectance (dashed line) of all 3 frequency points is around 30%, while the transmittance (solid line) is significantly low in the e-3 (1-4GHz), e-41 (23-33GHz), and e-131 (95-105GHz) level.

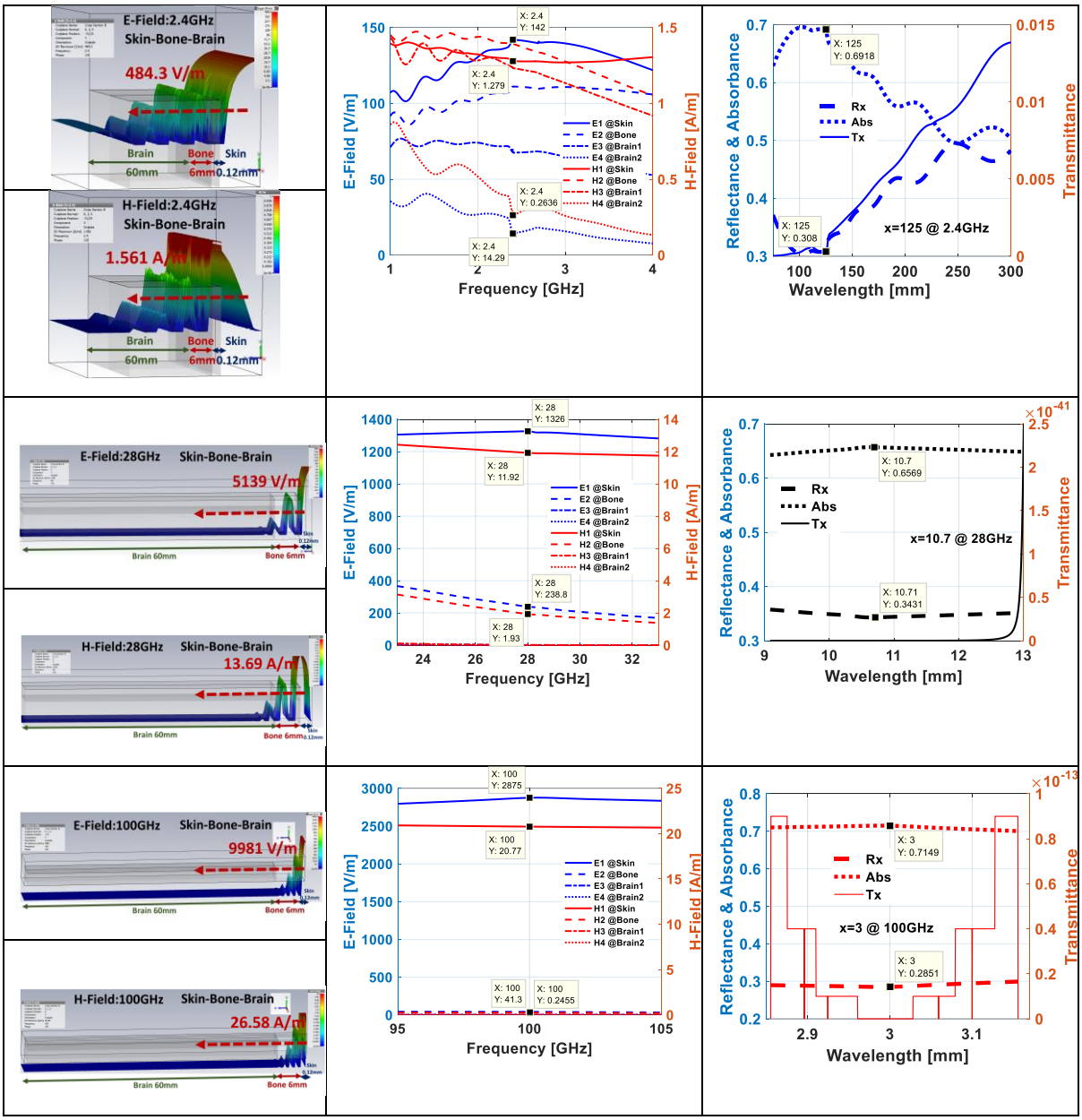

Figure 10. Left: E-and H-fields: 3D center-cut plane through a layer of 0.12mm skin, 0.6mm bone and 60mm brain skin-bone-brain layer in 1-4GHz, 23-33GHz, and 95-105GHz ranges. Middle: E- and H-fields collected at 0.06mm@skin, 3.06mm@bone, 9.06mm@brain1, and 36.06mm@brain2. Right: Reflectance (dashed), absorbance (dotted), and transmittance (solid) of the organ layer in the 3 frequency ranges.

5. Conclusion

Eight human organ and tissue models (blood, brain, breast, eye bulb, heart, kidney, liver and lung), while tested with electromagnetic excitation from 2.4GHz and 28GHz dipole antennas, and 95-105GHz waveguide ports, show that the wavelength of the E- and H-fields propagating inside the models is shortened or the wave frequency is accelerating, approximately 5-8 times. The lowest propagation frequency is found in the lung model, where the permittivity and conductivity are lowest among those of the eight studied models. The E-field intensity boosts significantly as the EM source frequency increases,

approximately 10 times between 2.4GHz and 28GHz. The E-field intensity (from 95GHz to 105GHz radiation) rises from 3.89% (in brain) to 4.86% (in liver). The field intensity dramatically decreases as the wave propagates passing the model, indicating high wave attenuation from the material absorption.

The EM absorbance is found to be greater than 60% in all 14 organ and tissue models. At 100GHz, the bone (83.01%), urinary bladder wall (82.95%), lung (80.02%), liver (68.18%), brain (66.18%), and eye bulb (64.46%) present the highest absorbance level. The absorbance increases significantly as the frequency increases, for instance, 43.78% at 2.4GHz, 51.95% at 28GHz, and 66.16% at 100GHz in the brain model. The transmittance in all models is below e-20 level. At all three operating frequencies: 2.4GHz, 28GHz, and 100GHz, the E- and H-fields vanish before passing through the brain layer of the Skin-Bone-Brain layered model. The overall layer absorbance is greatly elevated at all 3 frequencies: 69.18% at 2.4GHz, 65.69% at 28GHz, and 71.49% at 100GHz. The reflectance is around 30%, while the transmittance is significantly low. The scattering behavior and multiple absorbing possibility is observed. The absorbance is inversely proportional to the permittivity and conductivity of human organs and tissues. There is no clear correlation between the EM absorbance and heat transfer and generation rate. The models confirm that the higher the frequency, the greater the attenuation. Penetration is therefore reduced with increasing frequency. However, on the other hand, the absorption level increases with frequency. The results quantitatively validate the classic effects of the increase in frequency in terms of penetration and dissipation in human tissues and organs.

Further study of the EM radiation and propagation, either on specific complete human parts, for example an eye bulb with cornea, anterior chamber, pupil, iris, lens, ciliary and vitreous body, macular, retina, choroid and optic nerve, or the whole human body, will definitely provide more insight and correlation of the EM radiation and its effects amid all human organs.

Acknowledgements: This work is supported by NSF ADVANCE Grant (1209210) at the University of Texas Rio Grande Valley. NW thanks to Patricia Briea, environmental engineer, for the fruitful discussion on RF radiation and regulations.

References

1. https://standards.ieee.org/standard/521-2002.html IEEE 521-2002 IEEE Standard Letter Designations for Radar-Frequency Bands (accessed on 1 September 2020).
2. https://www.itu.int/pub/R-REG-RR International Telecommunication Union´s Radio Regulations (2012) (accessed on 1 September 2020).
3. https://www.cisco.com/c/m/en_us/solutions/service-provider/visual-networking-index.html (accessed on 1 September 2020).
4. Pihkola, H., Hongisto, M., Apilo, O., Lasanen, M. 2018. Evaluating the energy consumption of mobile data transfer—from technology development to consumer behaviour and life cycle thinking. Sustainability 10, 2494.
5. Coroama, V. C.; Schien, D.; Preist, C.; Hilty, L. M. 2015. The energy intensity of the internet: home and access networks. in ICT innovations for sustainability. Advances in Intelligent Systems and Computing. Springer International Publishing 2015, 310, pp. 137–155.
6. Norman, T. 2014. integrated security systems design, 2nd edition.
7. Ferguson, R.S., Williams, T. 1993. Safety and EMC in telecommunications engineer's reference book.
8. https://www.fcc.gov/sites/default/files/human_exposure_to_radio_frequency_fields_-_guidelines_for_cellular_antenna_sites.pdf (accessed on 1 September 2020).
9. Stutzman, W.L., Thiele, G.A. 2012. Antenna theory and design. Wiley. 3rd edition.
10. https://www.fda.gov/radiation-emitting-products/resources-you-radiation-emitting-products/microwave-oven-radiation A Federal standard: 21 CFR 1030.10 (accessed on 1 September 2020)..

11. Fleischman, E., Smith, R.E., Multari, N. 2008. Networked local area networks in aircraft: safety, security, and certification issues, and initial acceptance criteria (Phases 1 and 2). U.S. DOT, Federal Aviation Administration.
12. Whetten, F.L., Soroker, A., Whetten, D.A., Beggs, J.H. 2005. Wireless local area network performance inside aircraft passenger cabins. NASA/TP-2005-213763.
13. Serio, A.D. et al. 2018. Potential of sub-GHz wireless for future IoT wearables and design of compact 915 MHz antenna. Sensors 18, 22.
14. Bandara, P., Carpenter, D.O. 2018. Planetary electromagnetic pollution: it is time to assess its impact. www.thelancet.com/planetary-health 2, 512-524.
15. Lin, J.C. 2016. Human exposure to RF, microwave, and millimeter-wave electromagnetic radiation [Health Effects]. IEEE Microwave Magazine 17, 32-36.
16. Fernandez-Garcia, R., Gil, I. 2017. Measurement of the environmental broadband electromagnetic waves in a mid-size European city. Environ. Res. 158, 768-772.
17. Fernandez-Garcia, R., Gil, I. 2019. Validation of potential effects on human health of in vivo experimental models studied in rats exposed to sub-thermal radiofrequency. Possible health risks due to the interaction of electromagnetic pollution and environmental particles. IEEE Access 7, 79186-79198.
18. Kalic, G., Bojic, I., Kusek, M. 2012. Energy consumption in android phones when using wireless communication technologies. IEEE Proceedings of the 35th International Convention MIPRO.
19. Perrucci, G. P., Fitzek, F. H. P., Widmer, J. 2011. Survey on energy consumption entities on the smartphone platform. 2011 IEEE 73rd Vehicular Technology Conference.
20. https://ceet.unimelb.edu.au/publications/ceet-white-paper-wireless-cloud.pdf The Power of Wireless Cloud. ceet- Centre for energy-efficient telecommunications Bell Labs and University of Melbourne (2012). (accessed on 1 September 2020).
21. https://www.scienceabc.com/innovation/what-is-the-range-of-bluetooth-and-how-can-it-be-extended.html (accessed on 1 September 2020).
22. https://www.radiologyinfo.org/en/info.cfm?pg=safety-mr Magnetic Resonance Imaging (MRI) Safety. (accessed on 1 September 2020).
23. Bhargava, D., Leeprechanon, N., Rattanadecho, P., Wessapan, T. 2019. Specific absorption rate and temperature elevation in the human head due to overexposure to mobile phone radiation with different usage patterns. International Journal of Heat and Mass Transfer 130, 1178–1188.
24. Wessapan, T. and Rattanadecho, P. 2018. Temperature induced in human organs due to near-field and far-field electromagnetic exposure effects. International Journal of Heat and Mass Transfer 119, 65–76.
25. Wessapan, T. and Rattanadecho, P. 2016. Temperature induced in the testicular and related tissues due to electromagnetic fields exposure at 900 MHz and 1800 MHz. International Journal of Heat and Mass Transfer 102, 1130–1140.
26. https://www.who.int/health-topics/electromagnetic-fields#tab=tab_1 Electromagnetic fields. (accessed on 1 September 2020).
27. Kim, J.H., Lee, J.K., Kim, H.G., Kim, K.B., Kim, H.R. 2019. Possible effects of radio frequency electromagnetic field exposure on central nerve system. Biomol. Ther. 27, 3, 265-275.
28. Altun, G., Deniz, Ø.G., Yurt, K.K., Davis, D., Kaplan, S. 2018. Effects of mobile phone exposure on metabolomics in the male and female reproductive systems. Environ. Res. 167, 700-707.
29. Gruber, M.J., Palmquist, E., Nordin, S. 2018. Characteristics of perceived electromagnetic hypersensitivity in the general population. Scand. J. Psychol. 59, 422-427.
30. Kivrak, E.G., Yurt, K.K., Kaplan, A., Alkan, A., Altun, G. 2017. Effects of electromagnetic fields exposure on the antioxidant defense system. J. of Microscopy and Ultrastructure 5, 167-176.
31. Johansson, O., Redmayne, M. 2016. Exacerbation of demyelinating syndrome after exposure to wireless modem with public hotspot. Electromagn. Biol. Med. 35, 393-397.
32. Danker-Hopfe, H., Dorn, H., Bolz, T., Peter, A., Hansen, M.-L., Eggert, T., Sauter, C. 2016. Effects of mobile phone exposure (GSM 900 and WCDMA/UMTS) on polysomnography-based sleep quality: an intra- and inter-individual perspective. Environ. Res. 145, 50-60.

33. Kazemi, E. et al. 2015. Effect of 900 MHz electromagnetic radiation on the induction of ROS in human peripheral blood mononuclear cells. J. Biomed. Phys. Eng. 5, 105-114.
34. Ohtani, S. et al. 2015. The effects of radio-frequency electromagnetic fields on T cell function during development. J. Radiat. Res. 56, 467-474.
35. Singh, S., Kapoor, N. 2014. Health Implication of electromagnetic fields, mechanisms of actions, and research needs. Adv. in Biology 198609, 1-24.
36. Benson, V.S., Pirie, K., Schuz, J., Reeves, G.K., Beral, V., Green, J. 2013. Mobile phone use and risk of brain neoplasms and other cancers: prospective study. Int. J. Epidemiol. 42, 792-802.
37. Baan, R., Grosse, Y., Lauby-Secretan, B., El Ghissassi, F., Bouvard, V., Benbrahim-Tallaa, L., Guha, N., Islami, F., Galichet, L., Straif, K. 2011. Carcinogenicity of radiofrequency electromagnetic fields. Lancet Oncol. 12, 624-626.
38. Elliott, P., Toledano, M. B., Bennett, J., Beale, L., De Hoogh, K., Best, N., Briggs, D.J. 2010. Mobile phone base stations and early childhood cancers: case-control study. BMJ 340, c3077.
39. Phillips, J.L., Singh, N.P., Lai, H. 2009. Electromagnetic fields and DNA damage. Pathophysiology 16, 79-88.
40. Abdel-Rassoul, G. et al. 2007. Neurobehavioral effects among inhabitants around mobile phone base stations. Neurotoxicology 28, 434-440.
41. Hardell, L., Carlberg, M., Hansson Mild, K. 2005. Use of cellular telephones and brain tumor risk in urban and rural areas. Occup. Environ. Med. 62, 390-394.
42. Ahlbom, A., Feychting, M. 2003. Electromagnetic radiation. British Medical Bulletin, 68, pp. 157-165.
43. Pall, M.L. 2018. Wi-Fi is an important threat to human health. Environ. Res. 164, 406-416.
44. Sonsilphong, A., Wongkasem N. 2014. Light-weight radiation protection by non-lead materials in x-ray regimes. Proceedings ICEAA – IEEE APWC 2014.
45. https://www.3ds.com/products-services/simulia/products/cst-studio-suite/ CST Studio Suites.
46. Mitchell, H.H., Hamilton, T.S., Steggerda, F.R., Bean, H.W. 1945. The chemical composition of the adult human body and its bearing on the biochemistry of growth. J. of Biological Chemistry 158, 625-637.
47. https://itis.swiss/virtual-population/tissue-properties/database/heat-generation-rate/ (accessed on 1 September 2020).
48. Gabriel, C. 1996. Compilation of the dielectric properties of body tissues at RF and microwave frequencies. U.S. Air Force Report AFOSR-TR-96.
49. Tsubaki, S., Hayakawa, S., Ueda, T., Mitani, T., Suzuki, E., Fujii, S., Wada, Y. 2018. Proton-enhanced dielectric properties of polyoxometalates in water under radio-frequency electromagnetic waves. Materials 11, 1202.
50. Nie, Y.M., Liang, S., Yu, W.D., Yuan, H., Yan, J. 2018. Microwave-assisted preparation and characterization of a polyoxometalate-based inorganic 2D framework anode for enhancing lithium-ion battery performance. Chem. Asian J. 13, 1199–1205.
51. Mingos, D.M.P., Baghurst, D. 1991. Applications of microwave dielectric heating effects to synthetic problems in chemistry. Chem. Soc. Rev. 20, 1–47.
52. Gabriel, C., Gabriel, S., Grant, E.H., Halstead, B.S.J., Mingos, D.M.P. 1998. Dielectric parameters relevant to microwave dielectric heating. Chem. Soc. Rev. 27, 213–223.
53. Buchner, R., Hefter, G. 2009. Interaction and dynamics in electrolyte solutions by dielectric spectroscopy. Phys. Chem. Chem. Phys. 11, 8984–8999.
54. Frezza, F., Mangini, F., 2017. Tedeschi N. Introduction to electromagnetic scattering: tutorial. J. of the Opt. Soc. of America A 35, 1, 163-173.
55. Lorenz, L. 1890. Videnskabernes Selskab Skrifter, 6, 142.
56. Mie, G. 1908. Beiträge zur Optik trüber medien, speziell kollidaler Metallösungen. Ann. Phys. 330, 377-445.
57. Tzarouchis, D.; Sihvola, 2018. A. Light scattering by a dielectric sphere: perspectives on the Mie resonances. Applied Sciences 8, 184, 1-22.